Reconstruction of correlation-driven electron-hole dynamics by high-harmonic-generation spectroscopy

Jonathan Leeuwenburgh,[1] Bridgette Cooper,[1] Vitali Averbukh,[1] Jonathan P. Marangos,[1] and Misha Ivanov[1,2]
[1]*Blackett Laboratory, Imperial College London, London SW7 2AZ, United Kingdom*
[2]*Max Born Institute, 12489 Berlin Adlershof, Germany*
(Received 1 July 2014; published 29 September 2014)

We present detailed analysis of the recently proposed technique of high-order-harmonic generation spectroscopy of correlation-driven electron hole dynamics in atoms and molecules. This novel technique resolves Auger-type processes with attosecond-scale resolution by clocking the decay process with high-harmonic generation. The harmonic generation is driven by an attosecond, XUV pump pulse and a long-duration, infrared pulse. We present the strong-field-approximation-based theory of such an XUV-initiated high-order-harmonic generation process. We detail different ways of recovering the hole survival probability by altering experimental parameters to change the time-energy mapping of the harmonics. The various reconstruction methods are then simulated for $M_{4,5}NN$ Auger decay in krypton and molecular-orbital breakdown dynamics in *trans*-butadiene and propanal.

DOI: 10.1103/PhysRevA.90.033426 PACS number(s): 32.80.Hd, 32.80.Rm, 42.65.Ky, 42.62.Fi

I. INTRODUCTION

Resolving ultrafast hole dynamics induced by photoionization and driven by electron correlation is one of the key objectives of attosecond spectroscopy [1]. Previous techniques used to time-resolve ultrafast electronic dynamics generally fall into three separate groups.

The first group combines attosecond-scale pump pulses with longer-duration infrared (IR) probe pulses in "pump-probe" configurations. Changing the delay between the extreme ultraviolet (XUV) pump pulse and the IR pulse leads to a variation in the yield of different fragmentation products. The variation in yield has been used to study both shake-up dynamics [2] and Auger cascades [3,4] in atoms with femtosecond resolution, and hole migration in phenylalanine [5] on the time scale of tens of femtoseconds (where nuclear dynamics is expected to play a major role). Very recently, extension of this technique to few-femtosecond dynamics has been attempted [6]. However, the resolution of this method is limited by the durations of the two pulses and the technique cannot be readily extended to attosecond dynamics.

The second common group also uses attosecond pump pulses with longer-duration IR or near-IR pulses in so-called "streaking" experiments [7]. This technique has been applied to Auger processes wherein an excited-state ion decays via the emission of another electron to leave a doubly ionized atom, e.g., Auger decay in krypton [7], and shake-up [8] and postcollision interaction processes [9]. Streaking experiments require emission of a secondary electron to accelerate and detect. Streaking techniques are therefore limited in that they require the energy of the ionized state to be above the double-ionization threshold.

The final group of techniques resolves hole dynamics using high-order-harmonic spectroscopy [10]. High-harmonic generation (HHG) is a process wherein a strong infrared field ionizes an atom or a molecule, accelerates the photoelectron, and drives it back into the parent atom at some later time. At this time the photoelectron may recombine with the hole left in the parent atom or molecule and emit a photon with energy corresponding to the sum of the energy of the electron and the ionization potential of the initial state. High-order-harmonic spectroscopy typically relies upon strong-field (tunnel) ionization in the first step of the high-harmonic-generation process. As a direct consequence, the initial hole created by ionization and the subsequent hole dynamics are limited to the outer valence orbitals of the system. This is also the case in recent proposals to resolve hole oscillations via measurement of the emitted IR photons [11].

As a result of their limitations, none of these techniques is tailored to resolving the rich dynamics that results from ionization from orbitals between the outer valence and the double-ionization threshold [12], which may not be accompanied by the emission of a secondary electron. Sudden ionization from these inner-valence states results in complex dynamics as several eigenstates of the ion are coherently populated [13]. In the inner-valence energy region of polyatomic molecules, these eigenstates are typically composed of one-hole configurations (1h) mixed with a large proportion of two-hole–one-particle configurations (2h1p); this regime is known as molecular-orbital breakdown [14]. The electron population therefore oscillates between the initial one-hole configuration and two-hole–one-particle configurations. Qualitatively, this decay can be understood as an Auger-type transition into bound (e.g., Rydberg) states instead of the continuum [15]. In contrast to exponential Auger decay [16], these bound-bound transitions lead to nonexponential behavior of the hole survival probability [12]. Recently, a technique to measure such hole dynamics via single-photon laser-enabled Auger decay has been proposed [17], but has not yet been realized experimentally.

Our HHG spectroscopic [18] technique combines the strengths of HHG spectroscopy and streaking methods in that it can time-resolve both subfemtosecond Auger-type core dynamics and inner-valence hole dynamics where no secondary electron is emitted. For this technique, a pump-probe configuration where the atom or molecule is ionized by an extreme ultraviolet, subfemtosecond pulse is adopted. After ionization the produced photoelectron is accelerated

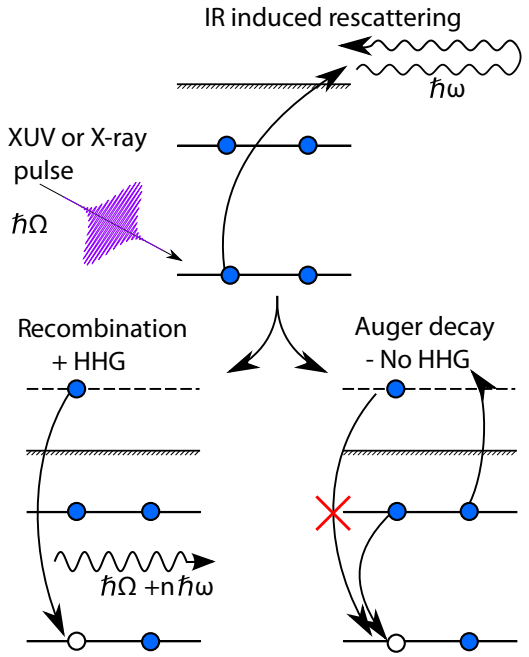

FIG. 1. (Color online) Shows the scheme by which our proposed technique works. Both the XIHHG and the Auger process compete for the hole formed by the XUV pulse; subsequently, the longer the photoelectron spends in the continuum the less likely it is to recombine and emit a high-harmonic photon.

by an IR field back into the parent system where it can probe the hole population (Fig. 1). If the initial hole is present, the electron may recombine resulting in coherent emission of so-called XUV-initiated high-harmonic generation (XIHHG) [19–21]. If, however, the ion has decayed to any other state before the photoelectron returns to the core then the electron cannot recombine to form the same ground state and coherent emission at the corresponding frequency does not occur. Consequently, in the case of monotonic decay, e.g., exponential decay, the longer the photoelectron spends in the continuum the less likely it is to contribute to the XIHHG radiation.

The present paper analyzes in further detail the scheme proposed in [18] and provides a description of several different methods of reconstructing the decay with a discussion of the differing experimental difficulties and differing requirements on prior knowledge of the system. The structure of the paper is as follows. Section II describes the theory behind our spectroscopic technique, Sec. III describes the mapping between the harmonic frequency and the excursion time, Sec. IV provides background on the specific examples of Auger decay and molecular orbital breakdown on which we focus, Secs. V and VI detail the different techniques to reconstruct the hole survival probability, and ultimately Sec. VII concludes the paper.

II. THEORY

We model the spectroscopy using the S-matrix formalism. This approach to XIHHG starts with the Hamiltonian

$$\hat{H} = \hat{H}_A + \hat{V}_L + \hat{V}_X, \tag{1}$$

where $\hat{H}_A$ is the atomic (molecular) Hamiltonian and includes the electron-electron repulsion and the core potential, $\hat{V}_X$ is the potential resulting from the XUV pulse, and $\hat{V}_L$ is the potential due to the IR field. The integral S-matrix form of the time-dependent Schrödinger equation (TDSE) [22] is (atomic units are used throughout this paper)

$$|\Psi(t)\rangle = -i\int^t dt'\left[e^{-i\int_{t'}^t \hat{H}(t'')dt''}\right][\hat{V}_X(t') + \hat{V}_L(t')] \times \left[e^{-i\int^{t'}\hat{H}_A(t'')dt''}\right]|g\rangle + e^{-i\int^t \hat{H}_A dt''}|g\rangle. \tag{2}$$

Here the state $|g\rangle$ represents the ground state. The first term in Eq. (2) corresponds to the part of the wave function that is in an excited state. The second term corresponds to the part of the wave function that remains in the ground state and ensures that at an initial time the system is in the ground state $|g\rangle$. The validity of this equation is easily verified by differentiation with respect to time and comparison with the TDSE. We can also write the equation in the form

$$|\Psi(t)\rangle = |\Psi_X(t)\rangle + |\Psi_g(t)\rangle, \tag{3}$$

where the first and second terms of this equation correspond to the first and second terms in Eq. (2), respectively. We now make several key assumptions. First, we assume that the IR field has a negligible effect on the ground state due to the deeply bound nature of the core electrons. This is an approximation commonly used in the interpretation of streaking experiments [7]. Second, we assume that the XUV field does not interact with the continuum photoelectron. This is reasonable as the ponderomotive energy of the XUV field will be much lower than that of the IR field, as the XUV frequency is much higher and the XUV intensity much lower that the IR field parameters. We also neglect the effect of the atomic potential compared to that of the IR field on the photoelectron. This is the basis of the Strong Field Approximation (SFA) [23] and is similar to the quantitative rescattering theory of strong-field ionization in IR fields [24]. The validity of this assumption in the case of XUV ionization in the IR field and the importance of the Coulomb-laser coupling [25] have been analyzed in Ref. [26]. The core is, however, accounted for in the photorecombination amplitude. Finally we assume that the ground-state depletion is negligible; this is also a common approximation for calculating the HHG spectra [23].

As a result of these approximations we rewrite Eq. (2) as

$$|\Psi(t)\rangle = -i\int^t dt' e^{-i\int_{t'}^t(\hat{H}_A+\hat{V}_L)dt''}\hat{V}_X(t')e^{-iE_g t'}|g\rangle + e^{-iE_g t}|g\rangle, \tag{4}$$

where we have implicitly used the fact that the evolution of the ground state under the atomic Hamiltonian is given by

$$e^{-i\int^t \hat{H}_A dt''}|g\rangle = e^{-iE_g t}|g\rangle. \tag{5}$$

At this point it should be noted that expressions obtained through the SFA, like the equation above, are general in that they can be factorized into the product of three amplitudes; ionization, propagation, and recombination. A quantitative description of high-harmonic processes can be obtained by using accurate ionization and recombination amplitudes,

e.g., by using the R-matrix [27] or algebraic diagrammatic construction formalism [28].

In order to calculate the spectrum we calculate the dipole moment $\tilde{\mathbf{d}}(t)$:

$$\begin{aligned}\tilde{\mathbf{d}}(t) &= \langle\Psi(t)|\hat{\mathbf{x}}|\Psi(t)\rangle \\ &= \langle\Psi_X(t)|\hat{\mathbf{x}}|\Psi_X(t)\rangle + \langle\Psi_g(t)|\hat{\mathbf{x}}|\Psi_g(t)\rangle \\ &\quad + 2\mathrm{Re}[\langle\Psi_X(t)|\hat{\mathbf{x}}|\Psi_g(t)\rangle]. \end{aligned} \tag{6}$$

Here $\hat{\mathbf{x}}$ represents the position operator. The first term in this equation corresponds to transitions between the continuum states. We may neglect this term as the probability of excitation is very small and the corresponding frequencies are much lower than for the continuum-ground transitions. The second term, i.e., the permanent dipole moment of the ground state, is not time dependent and may be neglected. We therefore need only consider the cross term given by

$$\mathbf{d}(t) = -i\int^t dt'\langle g|\hat{\mathbf{x}}e^{-i\int_{t'}^t[\hat{H}_A+\hat{V}_L(t'')]dt''}\hat{V}_X(t')e^{iE_g(t-t')}|g\rangle. \tag{7}$$

Let both the XUV and the IR fields be spatially homogeneous such that the relations between the potentials and the field strength are

$$\begin{aligned}\hat{V}_X(t') &= -\hat{\mathbf{x}}\cdot\mathbf{E}_X(t'), \\ \hat{V}_L(t') &= -\hat{\mathbf{x}}\cdot\mathbf{E}_L(t'). \end{aligned} \tag{8}$$

We now insert the identity in terms of all excited one-hole configurations of the ion $|\chi_n\rangle$ and continuum Volkov states labeled by the canonical momentum $|\mathbf{p}\rangle$ for the continuum electron,

$$\begin{aligned}\mathbf{d}(t) = i\sum_n\int d\mathbf{p}\int^t dt'\langle g|\hat{\mathbf{x}}e^{-i\int_{t'}^t[\hat{H}_A+\hat{V}_L(t'')]dt''} \\ \times|\chi_n,\mathbf{p}+\mathbf{A}(t')\rangle\langle\chi_n,\mathbf{p}+\mathbf{A}(t')|\hat{\mathbf{x}}\cdot\mathbf{E}_X(t')e^{iE_g(t-t')}|g\rangle, \end{aligned} \tag{9}$$

where we have defined the vector potential to be

$$\mathbf{A}(t) = -\int_{-\infty}^t\mathbf{E}_L(t'')dt''. \tag{10}$$

The evolution of the excited ionic wave function is described as

$$\begin{aligned}&e^{-i\int_{t'}^t[\hat{H}_A+\hat{V}_L(t'')]dt''}|\chi_n(t'),\mathbf{p}+\mathbf{A}(t')\rangle \\ &= e^{-iE_{\chi_n}(t-t')}e^{-i/2\int_{t'}^t[\mathbf{p}+\mathbf{A}(t'')]^2dt''}|\chi_n(t-t'),\mathbf{p}+\mathbf{A}(t)\rangle. \end{aligned} \tag{11}$$

Here we have implicitly made two assumptions; first, that the core potential has no effect on the continuum electron, and second, that the IR field has no effect on the ionic dynamics. As a result of the second assumption the ionic wave function is a function only of the excursion time $t-t'$. The energy of the involved ionic eigenstates is defined as E_{χ_n} and the corresponding phase evolution is explicitly written separately from the evolution of the configuration $|\chi_n(t-t'),\mathbf{p}+\mathbf{A}(t)\rangle$. The rest of the wave packet evolution is implicit in the time dependence of $\chi_n(t-t')$.

We now consider only the contribution to the dipole moment from a single initial 1h configuration of the ion. That is, we assume that the single XUV photon ionization removes an electron from one specific molecular or atomic orbital. We therefore drop the subscript n and instead introduce $\mathbf{d}_\chi(t)$ to represent the spectrum resulting from a specific 1h initial configuration of the ion. Denoting the phase accumulated by the continuum electron as

$$\frac{1}{2}\int_{t'}^t[\mathbf{p}+\mathbf{A}(t'')]^2dt'' = S(t,t',\mathbf{p}), \tag{12}$$

we can write the 1h configuration specific dipole moment as

$$\begin{aligned}\mathbf{d}_\chi(t) = i\int d\mathbf{p}\int^t dt'\langle g|\hat{\mathbf{x}}|\chi(t-t'),\mathbf{p}+\mathbf{A}(t)\rangle e^{-iS(t,t',\mathbf{p})} \\ \times\mathbf{E}_X(t')\cdot\langle\chi,\mathbf{p}+\mathbf{A}(t')|\hat{\mathbf{x}}|g\rangle e^{-i(E_\chi-E_g)(t-t')}. \end{aligned} \tag{13}$$

We can express the time-evolved ionic wave function as

$$|\chi(t-t')\rangle = a(t-t')|\chi\rangle + \sum_i a_i(t-t')|\psi_i\rangle. \tag{14}$$

Here $|\chi\rangle$ represents the 1h configuration populated at the instant of ionization and $|\psi_i\rangle$ represents all other 2h1p configurations into which the 1h configuration evolves. The other 1h and higher-order configurations may be neglected as in Auger decay and molecular-orbital breakdown dynamics these are not significantly populated by the evolution. We may now write

$$\langle g|\hat{\mathbf{x}}|\psi_i,\mathbf{p}+\mathbf{A}(t)\rangle \approx 0; \tag{15}$$

this is because the single electron dipole operator cannot act upon the 2h1p (plus continuum electron) configurations to form the ground state of the neutral species. Such recombination proceeds via the overlap of the wave packet $|\chi(t,t')\rangle$ with the 1h configuration $|\chi\rangle$.The dipole matrix element corresponding to recombination therefore reduces to

$$\langle g|\hat{\mathbf{x}}|\chi(t-t'),\mathbf{p}+\mathbf{A}(t)\rangle = a(t-t')\langle g|\hat{\mathbf{x}}|\chi,\mathbf{p}+\mathbf{A}(t)\rangle.$$

The phase of $a(t-t')$ evolves slowly in comparison to the other exponential terms present in Eq. (13) and is neglected; this approximation is valid when the populated ionic eigenstates are relatively close in energy compared to the ponderomotive energy [10]. Rewriting the dipole transition matrices in the form

$$\langle\chi,\mathbf{p}+\mathbf{A}(t')|\hat{\mathbf{x}}|g\rangle = \mathbf{d}_\chi[\mathbf{p}+\mathbf{A}(t')] \tag{16}$$

for clarity, we rewrite the dipole moment as

$$\begin{aligned}\mathbf{d}_\chi(t) = -i\int d\mathbf{p}\int^t dt'a(t-t')e^{-iS(t,t',\mathbf{p})}e^{-iI_p(t-t')} \\ \times\mathbf{E}_X(t')\cdot\mathbf{d}_\chi[\mathbf{p}+\mathbf{A}(t')]\mathbf{d}_\chi^*[\mathbf{p}+\mathbf{A}(t)]+\mathrm{c.c.} \end{aligned} \tag{17}$$

Here we have defined the ionization potential as $I_p = E_\chi - E_g$. We may now make a saddle-point approximation in an approach analogous to that of Lewenstein *et al.* [23]. We consider the saddle-point integration over the canonical momentum $\mathbf{p}$ and solve for the stationary point in the canonical momentum,

$$\nabla_p S(t,t',\mathbf{p}_{st}) = 0, \quad \mathbf{p}_{st} = -\frac{1}{t-t'}\int_{t'}^t\mathbf{A}(t'')dt''. \tag{18}$$

In this way we arrive at

$$\mathbf{d}_\chi(t) = -i\int^t dt' a(t-t')\left(\frac{\pi}{\eta + i(t-t')/2}\right)^{3/2} \times \mathbf{E}_X(t')\cdot\mathbf{d}_\chi[\mathbf{p}_{st}+\mathbf{A}(t')]\mathbf{d}^*_\chi[\mathbf{p}_{st}+\mathbf{A}(t)] \times e^{-iS(t,t',\mathbf{p}_{st})-iI_p(t-t')} + \text{c.c.}, \quad (19)$$

where η is infinitesimal. It is Eq. (19) that is implemented to obtain the dipole moment throughout this article. The harmonic spectrum is then obtained by taking the Fourier transform of the dipole acceleration,

$$\mathbf{d}_\chi(\omega) = \mathcal{F}\{\mathbf{d}_\chi(t)\}, \quad (20)$$

$$I_\chi(\omega) = 4\omega^4\pi^2\alpha^2|\mathbf{d}_\chi(\omega)|^2. \quad (21)$$

The electric field is assumed to have the form

$$\mathbf{E}_{IR}(t) = E_0\cos(\omega_{IR}t)\hat{\mathbf{x}}. \quad (22)$$

The simulated ionizing XUV pulse is a Gaussian of the form

$$\mathbf{E}_X(t) = E_X\cos(\omega_X t)e^{-[(t-t_X)/\alpha]^2}\hat{\mathbf{x}}. \quad (23)$$

The absolute time delay between the peak of the IR cycle and the XUV enevelope peak is seen to be t_X. For the remainder of the article, we measure the delay in degrees of the IR cycle,

$$\phi_X = t_X/T\times 360^\circ. \quad (24)$$

Here T is the IR period. A simulated spectrum is shown for ionizing from the $3d$ subshell in krypton in Fig. 2 while varying the position of the ionizing pulse in the IR field, ϕ_X. The IR field is modeled with a wavelength of 2700 nm and an intensity of 5×10^{13} W/cm^2. The continuous-wave nature of the IR field is appropriate as we consider the case where only one ionizing XUV pulse is present. The XUV pulse is modeled with a full width at half maximum (FWHM) of 108 as and central frequency equal to the I_p of the $3d$ subshell (93 eV). The exact XUV intensity is unimportant in the linear ionization regime: the spectrum uniformly scales linearly with the XUV intensity. The IR field and XUV pulse have the same, linear, polarization.

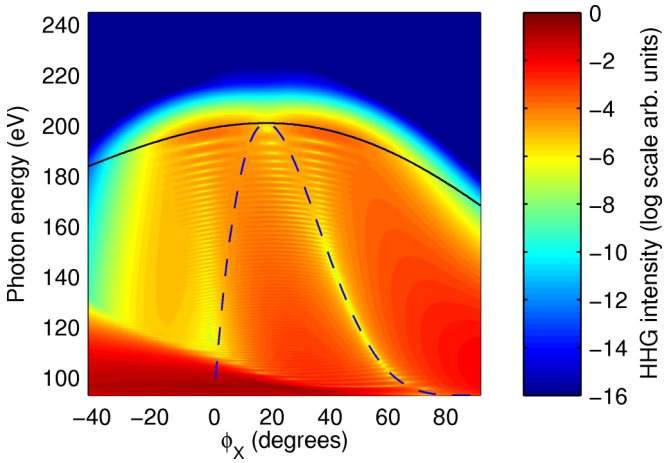

FIG. 2. (Color online) Shows simulated XUV-initiated high-harmonic spectra in krypton resulting from different IR-XUV delays. The black line indicates the classically calculated cutoff harmonic frequency. The blue dashed line indicates the minima in the spectra corresponding to ionization to zero initial velocity. Details of the simulation parameters can be found in the text.

We observe that the cutoff as a function of the XUV-IR delay approximately follows the classically calculated cutoff. In addition we note minima corresponding to ionization to zero initial kinetic energy. This is an artifact of the SFA and would not be observed if more realistic dipole transition matrix elements (DTMEs) were used. This confirms that, as expected, for $U_p \gg \omega_{IR}$ classical trajectories are the principal contributors to the spectrum. The high-intensity feature seen in the bottom left corner of Fig. 2 results from trajectories with very small excursion times. We now further examine Eq. (19) with a view to analytically establishing a map between the ionization time (t), excursion time ($\tau = t - t'$), and harmonic frequency (ω).

III. HIGH-HARMONIC TIME-ENERGY MAPPING

The key component of the method is a way of extracting the hole survival probability $|a(t-t')|^2$ from the spectrum. We need a way to relate a particular harmonic to a particular excursion time. With the goal of establishing such a time-energy mapping we now consider the harmonic spectrum

$$\mathbf{d}_\chi(\omega) = -i\int^t dt'\int_{-\infty}^{\infty} dt\, a(t-t')\left(\frac{\pi}{\eta + i(t-t')/2}\right)^{3/2} \times \mathbf{E}_X(t')\cdot\mathbf{d}_\chi[\mathbf{p}_{st}+\mathbf{A}(t')]\mathbf{d}^*_\chi[\mathbf{p}_{st}+\mathbf{A}(t)] \times e^{-iS(t,t',\mathbf{p}_{st})-iI_p(t-t')}e^{i\omega t} + \mathcal{F}(\text{c.c.}), \quad (25)$$

Where $\mathcal{F}$(c.c.) indicates the Fourier transform of the complex conjugate as indicated in Eq. (19), which in this case represents the negative frequencies in the spectrum. If we were to consider another saddle-point approximation, this time over t, we would obtain the conditions

$$\omega = \tfrac{1}{2}[\mathbf{p}_{st}(t_{st},t') + \mathbf{A}(t_{st})]^2 + I_p, \quad (26)$$

where we have explicitly written the dependence of $\mathbf{p}_{st}$ on t and t' for clarity. Physically, these saddle-point approximations have recovered the classical trajectory conditions; the classical equations of motion for the continuum electron are

$$\ddot{x} = -\mathbf{E}(t), \quad (27)$$

$$\dot{x} = \mathbf{v}(t') + \mathbf{A}(t) - \mathbf{A}(t') = \mathbf{p} + \mathbf{A}(t), \quad (28)$$

$$x = \int_{t'}^{t}[\mathbf{p} + \mathbf{A}(t'')]dt''. \quad (29)$$

The classical recombination condition that $\Delta x = 0$ is recovered from the first saddle-point approximation by comparison of Eqs. (29) to (18). Additionally our second saddle-point equation (26) states that recombination at time t emits a photon equal to the classical kinetic energy of the electron plus the ionization potential.

For sufficiently short XUV pulse durations the ionization time can be approximated by the time of the peak of the XUV pulse, i.e., $t' \approx t_X$. We can therefore use Eqs. (18) and (26) to retrieve a relation between the excursion time and the harmonic frequency as a function of the position of

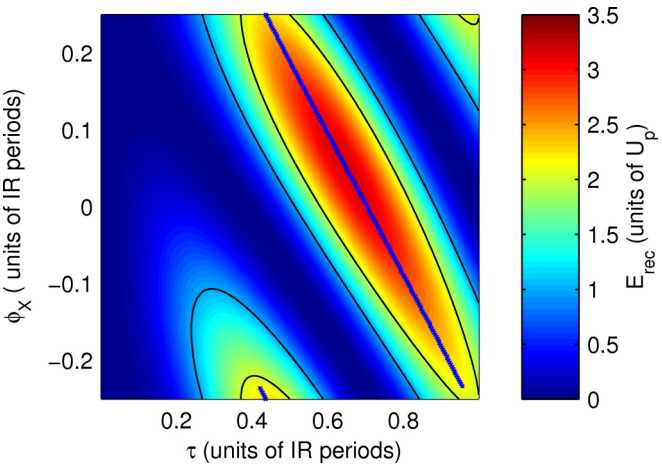

FIG. 3. (Color online) Shows the classically calculated recombination energy of the electron as a function of the position of the XUV within the IR field and the classical excursion time. The blue jagged line shows the position of the cutoff harmonic for each XUV position (this corresponds to the black line shown in Fig. 2). The solid black contours track the mapping for two different harmonic orders.

the XUV pulse (Fig. 3). Note that a specific time of ionization and a specific excursion time give rise to a single trajectory with a well-defined photon energy, whereas in general a specific harmonic energy can arise from a number of different trajectories (Fig. 4). Therefore, a single harmonic frequency does not correspond to a single classical trajectory. To avoid this problem, we concentrate on the cutoff harmonics (Fig. 3) or cases where the long trajectories have a weak contribution and may be neglected.

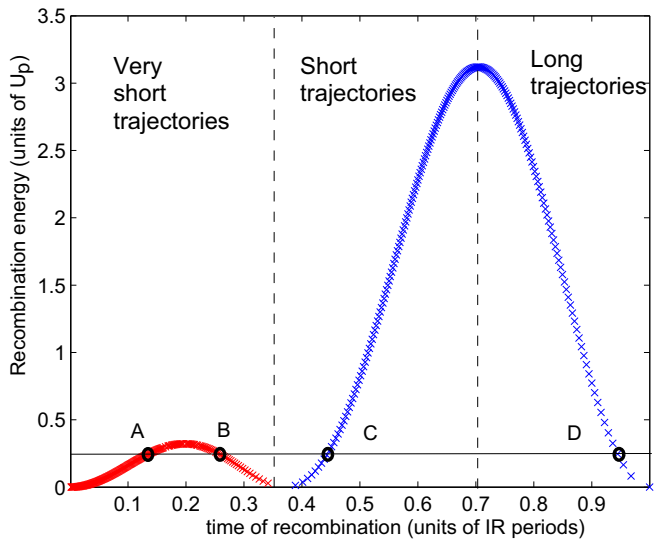

FIG. 4. (Color online) Shows the time of recombination against the recombination energy of the electron for the case where ionization occurs at the peak of the IR field ($\phi_X = 0$ of Fig. 3). It can be seen that some recombination energies correspond to four possible recombination times, two "very short" trajectories denoted by A and B, one "short" trajectory, and one "long" trajectory, denoted by C and D, respectively.

IV. AUGER DECAY AND MOLECULAR-ORBITAL BREAKDOWN DYNAMICS

In order to demonstrate possible methods of reconstruction of hole dynamics, let us concentrate on a few specific physical examples. The Auger-decay lifetime for krypton $M_{4,5}NN$ decay has been measured both by attosecond streaking [7] and by Auger electron spectroscopy [29] and is 7.48 ± 0.35 fs. We model the effect of this decay on our spectrum by setting

$$a(t - t') = e^{-(t-t')/(2\tau_L)}, \tag{30}$$

where τ_L is the Auger-decay lifetime.

In addition to this Auger decay, we also attempt to reconstruct the molecular-orbital breakdown dynamics for the $3A_g$ inner-valence hole in *trans*-butadiene and the $6A'$ inner-valence hole in propanal. The survival probabilities for these holes were obtained using the extended second-order algebraic diagrammatic construction [ADC(2)x] method [30] within the single-channel sudden approximation [13]. The single-electron Gaussian basis set [31,32] was chosen as correlation-consistent polarized valence triple zeta (cc-pCVTZ) with $3s3p$ diffuse functions for *trans*-butadiene and as correlation-consistent polarized valence double zeta (cc-pCVDZ) with $2s2p$ diffuse functions in propanal [33]. The grid numerical output from this procedure was then interpolated to give the survival probability for a given excursion time.

In the molecular cases we model ionization as occurring with the XUV polarization perpendicular to the plane of the molecule.

V. METHODS OF RECOVERING HOLE DECAY DYNAMICS ASSUMING KNOWN DTMES

In the following sections we show several different techniques for retrieving these electron dynamics from the high-harmonic spectra. These techniques all require accurate knowledge of the DTME for each system. Using the saddle-point approximation to pull out only the decay term from the integral over t in Eq. (25) we obtain

$$\begin{aligned}\mathbf{d}_\chi(\omega) \approx & -i \int^{t} a(t_{st} - t')dt' \int_{-\infty}^{\infty} dt \left(\frac{\pi}{\eta + i(t-t')/2}\right)^{3/2} \\ & \times \mathbf{E}_X(t') \cdot \mathbf{d}_\chi[\mathbf{p}_{st} + \mathbf{A}(t')]\mathbf{d}^*_\chi[\mathbf{p}_{st} + \mathbf{A}(t)] \\ & \times e^{-iS(t,t',\mathbf{p}_{st}) - iI_p(t-t')} e^{i\omega t},\end{aligned} \tag{31}$$

where the negative-frequency terms arising from the complex conjugate have been neglected for ease of reading. If the ionizing pulse is temporally short compared to the characteristic decay time, we may pull $a(t_{st} - t')$ out of the integral over t' to obtain

$$\begin{aligned}\mathbf{d}_\chi(\omega) \approx & -ia(t_{st} - t_X) \int_{-\infty}^{\infty} dt \int^{t} dt' \left(\frac{\pi}{\eta + i(t-t')/2}\right)^{3/2} \\ & \times \mathbf{E}_X(t') \cdot \mathbf{d}_\chi[\mathbf{p}_{st} + \mathbf{A}(t')]\mathbf{d}^*_\chi[\mathbf{p}_{st} + \mathbf{A}(t)] \\ & \times e^{-iS(t,t',\mathbf{p}_{st}) - iI_p(t-t')} e^{i\omega t},\end{aligned} \tag{32}$$

where t_X indicates the time at which the center of the XUV pulse occurs. Here the harmonic number ω, t_{st}, and t_X are

related by

$$\omega = \tfrac{1}{2}[\mathbf{p}_{st}(t_{st},t_X) + \mathbf{A}(t_{st})]^2 + I_p. \tag{33}$$

We now see that if the dipole transition matrix elements are known, we may calculate a theoretical dipole moment $\mathbf{d}_0(\omega)$ with $a(t_{st} - t_X) = 1$. The hole survival probability can then be extracted via

$$|a(t_{st} - t_X)|^2 \propto \left|\frac{\mathbf{d}_\chi(\omega)}{\mathbf{d}_0(\omega)}\right|^2 \propto \frac{I_\chi(\omega)}{I_0(\omega)}. \tag{34}$$

In the following sections we detail different methods of using this equation to recover the survival probability for a range of times.

A. Reconstruction from a single spectrum

The most immediate choice of reconstruction procedure for $a(t - t')$ is to note that, if we ignore the long trajectories, each harmonic corresponds to a single trajectory with a varying excursion time (Figs. 3 and 4). We expect that the short trajectories will phase match along the laser axis. To simulate the on-axis intensity we apply a cosine squared mask to the long trajectories such that trajectories corresponding to excursion times longer than the cutoff excursion time (τ_{co}) contribute less to the spectrum:

$$F(t - t' < \tau_{co}) = 1,$$
$$F(\tau_{co} < t - t' < \tau_{co} + 0.377T) = \cos^2\left(\frac{\pi}{2} \times \frac{t - t' - \tau_{co}}{0.377T}\right),$$
$$F(t - t' > \tau_{co} + 0.377T) = 0.$$

This filter, in addition to the exponential decay of the hole in the krypton case, often means that the long-trajectory contribution to the spectrum is negligible. In addition the DTME is often such that the longer trajectories are weaker as they require ionization to a greater initial kinetic energy; however, this need not be the case. We define the "population" of a trajectory due to the DTMEs to be

$$O(\omega) = \left|\frac{\mathbf{d}_\chi[\mathbf{p}_{st} + \mathbf{A}(t_X)]\mathbf{d}^*_\chi[\mathbf{p}_{st} + \mathbf{A}(t_{st})]}{(t_{st} - t_X)^3}\right|^2. \tag{35}$$

Provided the DTMEs are known, we can use a single experimental spectrum and one theoretical spectrum to investigate the hole population for a range of excursion times using Eq. (34).

The reconstructed Auger decay resulting from krypton $3d$ ionization is shown in Fig. 5. The XUV pulse was simulated to have a FWHM of 250 as and central frequency equal to the relevant I_p. The IR field is of a wavelength of 2700 nm and an intensity of 2×10^{13} W/cm^2. The IR-XUV delay in this case was such that $\phi_X = 90^\circ$; this delay was specifically chosen as longer trajectories are suppressed by the DTMEs.

This method of reconstruction provides excellent reconstruction of the survival probability for excursion times where the short trajectories have a much greater population than the long trajectories (for $\phi_X = 90^\circ$ between 1 and 4 fs). Note that as the long trajectories have a smaller contribution to the spectrum the short trajectories map out the decay. If the long trajectories had a greater contribution, they would reproduce

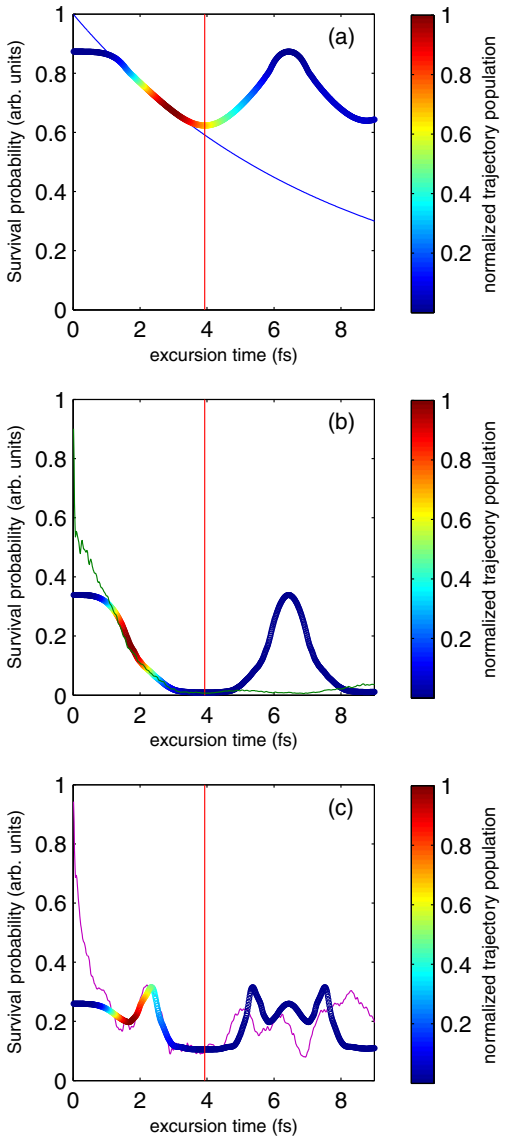

FIG. 5. (Color online) Shows the expected survival probability (solid lines) and reconstructed survival probability (circles) for (a) Auger decay in krypton and molecular-orbital breakdown dynamics in (b) propanal and (c) *trans*-butadiene. The reconstruction uses a single simulated spectrum and a purely theoretical spectrum where $a(t - t') = 1$, and uses the classical map to convert harmonic frequency to excursion time. The red vertical line corresponds to the cutoff excursion time; the population of a trajectory [as defined by Eq. (35)] is represented by the color of each point, with red points having greater population and blue points a weaker population.

the decay. The quality of the reconstruction deteriorates as the contribution from the long trajectories increases (i.e., approaching the cutoff); this is due to interference between the long and short trajectories. It is for this reason that harmonics corresponding to very low excursion times also do not reconstruct the decay; in this case the contributions from the very short trajectories mask the decay (Fig. 4).

Other disadvantages of this method are that it relies on detailed knowledge of the photoionization cross sections and

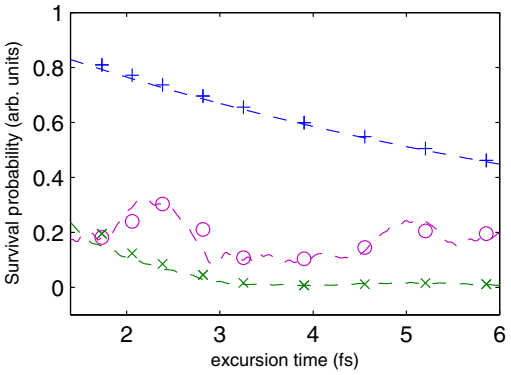

FIG. 6. (Color online) Shows the expected (dashed lines) and reconstructed (markers) survival probabilities of Auger dynamics in krypton (top, blue) and molecular-orbital dynamics in propanal (bottom, green) and *trans*-butadiene (middle, purple). The reconstruction uses nine spectra with different wavelengths of 800, 950, 1100, 1300, 1500, 1800, 2100, 2400, and 2700 nm (representing points from left to right), each corrected by a corresponding theoretical spectrum with $a(t-t')=1$.

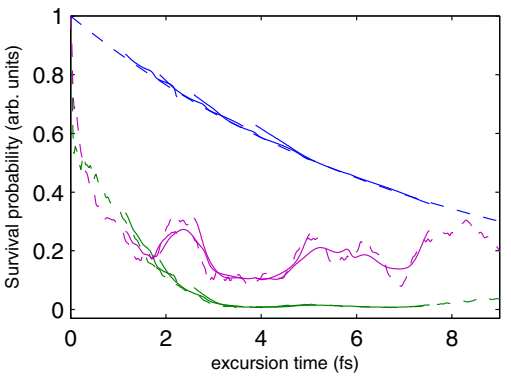

FIG. 7. (Color online) Shows the expected (dashed lines) and reconstructed (solid lines) survival probabilities for krypton (top, blue), propanal (bottom, green), and *trans*-butadiene (middle, purple). The reconstruction considers the cutoff harmonic intensity as the cutoff excursion time is varied by changing the XUV-IR delay. The cutoff intensity is corrected by a purely theoretical intensity where $a(t-t')=1$ to give the survival probability, and the classical map is used to convert the cutoff harmonic frequency to excursion time. The time domain for reconstruction is extended by performing the reconstruction using wavelengths of 800, 1300, 1800, and 2700 nm.

that phase-matching effects must uniform across the high-harmonic plateau. In addition it requires the experimental parameters and DTMEs be such that the short trajectories are much more populated than the long trajectories.

B. Reconstruction from varying wavelength

Another clear way to change the energy-time mapping is to perform multiple measurements at different IR wavelengths. Considering only the cutoff harmonic for each IR-XUV delay, there is only one trajectory and we need not worry about contributions from multiple trajectories. The reconstructed decay is shown in Fig. 6, where only the cutoff harmonics at $\approx 3.17U_p$ are used. An advantage of this technique is that the ultrafast XUV pulses need not be so temporally short. This is because irrespective of where in the IR cycle the XUV pulse is or ionization occurs, there is only one trajectory that leads to this maximum harmonic frequency. Provided the XUV pulse overlaps a phase of 17.9° in the IR cycle, the trajectory will be populated and will be unique with respect to the recombination energy. For these reconstructions we use an XUV pulse of FWHM 500 as and IR wavelengths of 800, 950, and 1100 nm at an intensity of 8×10^{13} W/cm^2, 1300, 1500, 1800, and 2100 nm at an intensity of 5×10^{13} W/cm^2, and 2400 and 2700 nm at an intensity of 2×10^{13} W/cm^2. This method recovers a lifetime of 7.35 fs for the Auger decay in krypton compared to the expected value of 7.48 fs.

This technique again requires knowledge of the DTMEs as the initial and final electron energies will vary with the wavelength. In addition this technique requires phase-matching and macroscopic effects to be the same for a given XUV-IR phase delay but with different wavelengths. Finally this method is particularly sensitive to changes in the wave packet spreading and the effect of the parent ion as the two compared trajectories will have very different excursion distances due to the changing ponderomotive energy U_p.

C. Reconstruction by varying XUV-IR delay

It is also possible to extract the survival probability by varying the position of the XUV pulse in the IR field (i.e., by varying ϕ_X). Varying ϕ_X leads to changes in the time-energy mapping between harmonic number and excursion time (Fig. 3). We now consider the cutoff harmonics as a function of ϕ_X (represented by the circles in Fig. 3). In contrast to the previous method, looking only at the cutoff harmonics has the advantage that there is only a contribution from a single, unique trajectory with a single excursion time. Correcting the spectral intensity via Eq. (34), we can reconstruct the survival probabilities as shown in in Fig. 7. In this case the reconstruction was performed using 800 nm IR at 8×10^{13} W/cm^2, 1300 and 1800 nm IR at 5×10^{13}W/cm^2, and 2700 nm IR at 2×10^{13} W/cm^2. In each case the XUV pulse was simulated to have a central frequency equal to the relevant I_p and a FWHM of 250 as.

VI. METHODS OF RECOVERING HOLE DECAY DYNAMICS WITHOUT KNOWLEDGE OF DTMES

The methods described so far have all utilized Eq. (34) and as a result have all required that the DTMEs be known for each system investigated. Returning to Eq. (34), we now use the saddle-point approximation to pull the DTMEs out of the integral over t;

$$\mathbf{d}_\chi(\omega) \approx -ia(t_{st}-t_X)\int_{-\infty}^{\infty} dt\ \mathbf{d}_\chi[\mathbf{p}_{st}+\mathbf{A}(t')] \times \mathbf{d}^*_\chi[\mathbf{p}_{st}+\mathbf{A}(t_{st})]\int^{t} dt' \left(\frac{\pi}{\eta+i(t-t')/2}\right)^{3/2} \times \mathbf{E}_X(t')e^{-iS(t,t',\mathbf{p}_{st})-iI_p(t-t')}e^{i\omega t}. \quad (36)$$

Additionally, if the dipole transition matrix elements are known to vary slowly we may also approximate the dipole

moment as

$$\mathbf{d}_\chi(\omega) \approx -i\, a(t_{st}-t_X)\mathbf{d}_\chi[\mathbf{p}_{st}+\mathbf{A}(t_X)]\mathbf{d}^*_\chi[\mathbf{p}_{st}+\mathbf{A}(t_{st})] \times \int_{-\infty}^{\infty} dt \int^{t} dt' \left(\frac{\pi}{\eta + i(t-t')/2}\right)^{3/2} \times \mathbf{E}_X(t') e^{-iS(t,t',\mathbf{p}_{st})-iI_p(t-t')} e^{i\omega t}. \quad (37)$$

The methods described in the rest of this section use this equation to remove the effects of the DTMEs on the spectra. This is achieved by comparing trajectories for which the excursion times are different but the values of the DTMEs are approximately the same.

A. DTME-independent reconstruction by varying XUV-IR delay

Varying the XUV-IR delay results in excellent reproduction of the survival probability when the DTMEs are known. However, if the DTMEs are not known we may still extract details of the decay process by exploiting an approximate symmetry in the high-harmonic process.

Considering the trajectory that gives the highest-order harmonics, it is noted that classically ionization occurs 17.9° from the peak of the IR field with an initial electron energy of zero, and recombination occurs ≈0.6 laser periods later with an electron energy equal to $3.17U_p$. If we now consider two times of ionization, one slightly above and the other slightly below this point, and in each case consider the trajectory that recombines with the greatest energy (given by the blue line in Fig. 3), it is observed that for a given recombination energy the initial velocities of the trajectories are approximately equal in magnitude and differ only in sign. There exist two trajectories that result in the same harmonic energy and begin with the same initial speed but occur at two different ionization times and have two different excursion times. We label these pairs of trajectories by their ionization times, which are inherently linked to the XUV-IR delay ϕ_X and ϕ'_X. Considering Eq. (37) we may extract the ratio of the survival probabilities,

$$Q(\phi_X,\phi'_X) \equiv \left|\frac{a[\tau_{co}(\phi_X)]}{a[\tau_{co}(\phi'_X)]}\right|^2 \approx \frac{I_\chi(\omega)P'(\omega)}{I'_\chi(\omega)P(\omega)}, \quad (38)$$

where the prime indicates that the XUV pulse is positioned to populate the trajectory with the shorter excursion time of the pair. The subscript *co* indicates that only the cutoff harmonic intensity is considered for each XUV-IR delay. The factor $P(\omega)$ corrects for the different population of trajectories by the XUV pulse,

$$P(\omega) = \left| \int_{-\infty}^{\infty} dt \int^{t} dt' \left(\frac{\pi}{\eta + i(t-t')/2}\right)^{3/2} \times \mathbf{E}_X(t') \cdot \hat{\boldsymbol{\epsilon}}\, e^{-iS(t,t',\mathbf{p}_{st})-iI_p(t-t')} e^{i\omega t} \right|^2. \quad (39)$$

Here $\hat{\boldsymbol{\epsilon}}$ is a unit vector in the direction of the polarization of the IR field. Using this method one is able to extract the Auger-decay lifetime in the case of exponential decay and extract qualitative details from nonmonotonic decay of the form seen in molecular-orbital breakdown dynamics. We simulate reconstruction using 2700 nm IR at 2×10^{13} W/cm^2 in the case of krypton and *trans*-butadiene and 1300 nm IR at 5×10^{13} W/cm^2 in the case of propanal (Fig. 8), and an XUV pulse of 250 as. This method of reconstruction gives an Auger lifetime of 8.19 fs for krypton and excellently reproduces the quasiexponential decay in propanal. The reconstruction of the relative survival probabilities in *trans*-butadiene is less well reproduced due to the quickly varying nature of the decay around 6 fs. However, in comparison to the results obtained for the exponential and quasiexponential decay, the reconstruction clearly shows that the survival probability is nonmonotonic in this case.

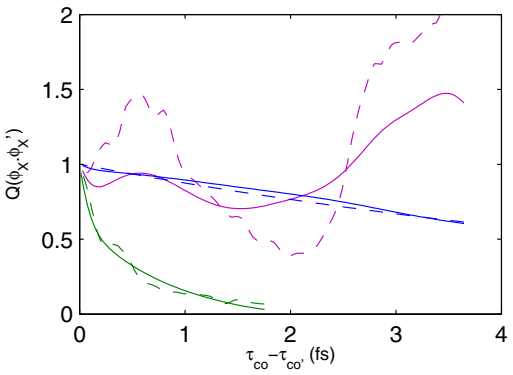

FIG. 8. (Color online) Shows the expected (dashed lines) and reconstructed (solid lines) survival probability ratios for krypton (blue), propanal (green), and *trans*-butadiene (purple). The reconstruction uses a range of different spectra each with different XUV-IR delays, and uses Eq. (38) to reconstruct the survival probability without knowledge of the DTMEs.

B. Reconstruction with constant ponderomotive energy

Considering Fig. 4, we see that if we hold the harmonic frequency constant and change the intensity, the excursion time associated with the harmonic changes. While reconstruction by altering the intensity is experimentally appealing, it is limited by a very small range of excursion times. Additionally we would again require that the long trajectories be significantly weaker than the short trajectories. If, however, the IR wavelength and intensity are varied in unison such that the ponderomotive energy is constant, reconstruction of the decay can be performed without knowledge of the DTMEs. Considering a single harmonic frequency, the initial and recombination electron energies remain constant while the excursion time associated with the harmonic changes. While experimentally challenging, this would completely remove the reliance on well-known photoionization and recombination cross sections. However, it would share the other disadvantages of the previous methods as it would be sensitive to macroscopic effects and the differences in the effects of the core potential due to the different excursion distances.

It should be noted that though the DTMEs need no longer be known, it is still required to adjust for the different population of trajectories by the XUV pulse. This is done by dividing the intensity by the correction factor $P(\omega)$. Note that the correction factor $P(\omega)$ does not assume or require prior knowledge of the DTMEs. The results from comparing the classical cutoff harmonic intensity for each XUV-IR delay for wavelengths of

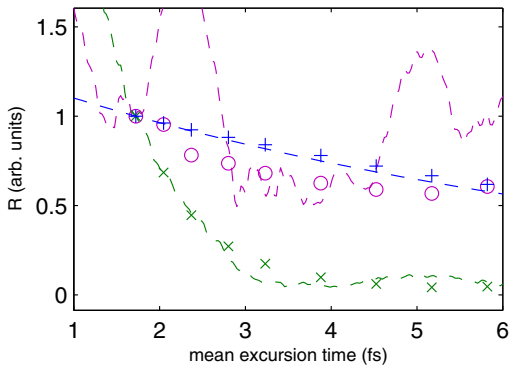

FIG. 9. (Color online) Shows the expected (dashed line) and reconstructed (markers) survival probabilities for Auger dynamics in krypton (top, blue) and molecular-orbital picture breakdown dynamics in propanal (bottom, green) and *trans*-butadiene (middle, purple). Both reconstructed and expected survival probabilities are normalized to equal unity at the earliest mean excursion time. The reconstruction uses nine spectra with different wavelengths but the same ponderomotive energy, each normalized by a theoretical spectrum to correct for the different population of trajectories according to Eq. (40). The wavelengths, listed in order from shortest mean excursion time to the longest, are 800, 950, 1100, 1300, 1500, 1800, 2100, 2400, and 2700 nm.

800, 950, 1100, 1300, 1500, 1800, 2100, 2400, and 2700 nm and constant U_p of 7.8 eV (corresponding to an IR intensity of 5×10^{13} W/cm^2 at 1300 nm) and an XUV pulse of FWHM 108 as are shown in Fig. 9. In this case we alter the XUV-IR delay ϕ_X and average the corrected intensity of the cutoff harmonics (represented by the solid black line in Fig. 2) over all ϕ_X; the classical excursion time is also averaged. The corrected intensity R in this case is is given by

$$R = \frac{1}{n}\sum_n \frac{I_{\chi,\omega_{IR}}\left(\omega,\phi_X^{(n)}\right)}{P_{\omega_{IR}}\left(\omega,\phi_X^{(n)}\right)}, \tag{40}$$

where n refers to the number of different spectra recorded at different $\phi_X^{(n)}$. An exponential fit to this method of reconstruction yields an Auger-decay lifetime of 8.55 fs in krypton compared to the expected value of 7.48 fs. As a consequence of the averaging involved in Eq. (40) we do not resolve the revivals in the survival probability for the case of *trans*-butadiene.

VII. CONCLUSIONS

We have demonstrated that HHG spectroscopy of correlation-driven hole dynamics is a versatile technique which can address both previously time-resolved Auger decay and previously unmeasured bound multielectron dynamics associated with the so-called orbital breakdown in molecules. We have outlined several methods of reconstructing the survival probability with differing experimental difficulties and differing requirements on *a priori* knowledge of the system. The first method of reconstruction requires the measurement of a single spectrum in addition to a reference simulated spectrum in which the decay does not occur. This method requires accurate photoionization and recombination cross sections in addition to characterization of phase-matching effects across the high-harmonic plateau. In addition, this method requires that the contributions from short and long trajectories can be distinguished, e.g., through macroscopic effects.

We have also shown two methods of reconstructing the decay by changing the XUV-IR delay. One of them requires reference simulated spectra but offers a larger reconstruction window and unambiguous, attosecond-resolution reconstruction of the survival probability. This method also requires phase-matching effects to be characterized across the plateau. The second method does not require explicit knowledge of the cross sections and is not sensitive to changes in the phase matching with respect to harmonic order. This latter method, however, gives only the relative survival probability between two excursion times, which limits its usefulness when reconstructing nonexponential decay.

Finally we have detailed two possible methods of reconstructing the survival probability by changing either the IR wavelength on its own or both the IR wavelength and intensity simultaneously. Changing the IR wavelength on its own allows us to use longer XUV pulses but does require accurate knowledge of the photoionization and recombination cross sections in addition to uniform phase-matching effects across the high-harmonic plateau. Varying the IR wavelength and intensity together has the advantage of not requiring prior knowledge of the cross sections and is not sensitive to changes in the phase matching with respect to harmonic order. However, this method cannot resolve the fast, oscillatory dynamics resulting from molecular-orbital picture breakdown in *trans*-butadiene.

We believe that varying the XUV-IR delay is the most advantageous and experimentally realizable method of those proposed in this article. For this reason we hope to stimulate experimental work in this area, in particular in the case of the Auger decay in krypton, where the results can be benchmarked against energy-domain and streaking measurements. In terms of further theoretical work to be carried out, macroscopic propagation of the XIHHG signal remains to be performed. In addition, incorporation of the effect of the core on the continuum electron through Coulomb-eikonal-Volkov wave functions in the continuum [26] will lead to more rigorous simulation of the very short trajectories.

ACKNOWLEDGMENTS

Fruitful discussions with Olga Smirnova are gratefully acknowledged. J.L. and V.A. acknowledge the financial support of the Engineering and Physical Sciences Research Council (EPSRC, U.K.) through the Career Acceleration Fellowship (Award No. EP/H003657/1). M.I., B.C., J.P.M., and V.A. acknowledge the financial support of the EPSRC through the Program Grant on Attosecond Dynamics (Award No. EP/I032517). M.I. and V.A. acknowledge the support of CORINF, a Marie Curie ITN of the European Union, Grant Agreement No. 264951. J.P.M. acknowledges the support of ERC Advanced Grant ASTEX Project No. 290467.

[1] F. Krausz and M. Ivanov, Rev. Mod. Phys. **81**, 163 (2009).
[2] M. Uiberacker, T. Uphues, M. Schultze, A. Verhoef, V. Yakovlev, M. Kling, J. Rauschenberger, N. Kabachnik, H. Schröder, M.Lezius, K. Kompa, H.-G. Muller, M. Vrakking, S. Hendel, U. Kleineberg, U. Heinzmann, M. Drescher, and F. Krausz, Nature (London) **446**, 627 (2007).
[3] T. Uphues, M. Schultze, M. F. Kling, M. Uiberacker, S. Hendel, U. Heinzmann, N. M. Kabachnik, and M. Drescher, New J. Phys. **10**, 025009 (2008).
[4] M. Krikunova, T. Maltezopoulos, A. Azima, M. Schlie, U. Frhling, H. Redlin, R. Kalms, S. Cunovic, N. M. Kabachnik, M. Wieland, and M. Drescher, New J. Phys. **11**, 123019 (2009).
[5] L. Belshaw, F. Calegari, M. J. Duffy, A. Trabattoni, L. Poletto, M. Nisoli, and J. B. Greenwood, J. Phys. Chem. Lett. **3**, 3751 (2012).
[6] F. Calegari (private communication).
[7] M. Drescher, M. Hentschel, R. Kienberger, M. Uiberacker, V. Yakovlev, A. Scrinzi, T. Westerwalbesloh, U. Kleineberg, U. Heinzmann, and F. Krausz, Nature (London) **419**, 803 (2002).
[8] A. Verhoef, A. Mitrofanov, M. Krikunova, N. M. Kabachnik, M. Drescher, and A. Baltuska, in *CLEO: 2013* (Optical Society of America, Washington, DC, 2013), p. QF2C.4.
[9] B. Schütte, S. Bauch, U. Frühling, M. Wieland, M. Gensch, E. Plönjes, T. Gaumnitz, A. Azima, M. Bonitz, and M. Drescher, Phys. Rev. Lett. **108**, 253003 (2012).
[10] O. Smirnova, Y. Mairesse, S. Patchkovskii, N. Dudovich, D. Villeneuve, P. Corkum, and M. Y. Ivanov, Nature (London) **460**, 972 (2009).
[11] A. I. Kuleff and L. S. Cederbaum, Phys. Rev. Lett. **106**, 053001 (2011).
[12] V. Averbukh, U. Saalmann, and J. M. Rost, Phys. Rev. Lett. **104**, 233002 (2010).
[13] T. Åberg, Phys. Rev. **156**, 35 (1967).
[14] L. Cederbaum, W. Domcke, J. Schirmer, and W. von Niessen, Adv. Chem. Phys. **65**, 115 (1986).
[15] J. Craigie, A. Hammad, B. Cooper, and V. Averbukh, J. Chem. Phys. **141**, 014105 (2014).
[16] B. Crasemann, *Atomic Inner-shell Processes: Ionization and Transition Probabilities* (Academic Press, New York, 1975).
[17] B. Cooper and V. Averbukh, Phys. Rev. Lett. **111**, 083004 (2013).
[18] J. Leeuwenburgh, B. Cooper, V. Averbukh, J. P. Marangos, and M. Ivanov, Phys. Rev. Lett. **111**, 123002 (2013).
[19] M. B. Gaarde, K. J. Schafer, A. Heinrich, J. Biegert, and U. Keller, Phys. Rev. A **72**, 013411 (2005).
[20] J. Biegert, A. Heinrich, C. Hauri, W. Kornelis, P. Schlup, M. Anscombe, K. Schafer, M. Gaarde, and U. Keller, Laser Phys. **15**, 899 (2005).
[21] G. Gademann, F. Kelkensberg, W. K. Siu, P. Johnsson, M. B. Gaarde, K. J. Schafer, and M. J. J. Vrakking, New J. Phys. **13**, 033002 (2011).
[22] A. Becker and F. H. M. Faisal, J. Phys. B **38**, R1 (2005).
[23] M. Lewenstein, P. Balcou, M. Y. Ivanov, A. L'Huillier, and P. B. Corkum, Phys. Rev. A **49**, 2117 (1994).
[24] Z. Chen, A.-T. Le, T. Morishita, and C. D. Lin, Phys. Rev. A **79**, 033409 (2009).
[25] O. Smirnova, A. S. Mouritzen, S. Patchkovskii, and M. Y. Ivanov, J. Phys. B **40**, F197 (2007).
[26] O. Smirnova, M. Spanner, and M. Y. Ivanov, J. Phys. B **39**, S323 (2006).
[27] A. G. Harvey and J. Tennyson, J. Phys. B **42**, 095101 (2009).
[28] M. Ruberti, R. Yun, K. Gokhberg, S. Kopelke, L. S. Cederbaum, F. Tarantelli, and V. Averbukh, J. Chem. Phys. **139**, 144107 (2013).
[29] M. Jurvansuu, A. Kivimäki, and S. Aksela, Phys. Rev. A **64**, 012502 (2001).
[30] A. B. Trofimov and J. Schirmer, J. Chem. Phys. **123**, 144115 (2005).
[31] K. L. Schuchardt, B. T. Didier, T. Elsethagen, L. Sun, V. Gurumoorthi, J. Chase, J. Li, and T. L. Windus, J. Chem. Inf. Model. **47**, 1045 (2007).
[32] D. Feller, J. Comput. Chem. **17**, 1571 (1996).
[33] K. Kaufmann, W. Baumeister, and M. Jungen, J. Phys. B **22**, 2223 (1989).